RESEARCH ARTICLE

An Astute Automaton Model for Objects Extraction Using Outer Totality Cellular Automata (OTCA)

SANDEEP KUMAR SHARMA[1], (Member, IEEE), **VIJAY SHANKAR SHARMA**[1], (Member, IEEE), **SHAKILA BASHEER**[2], **AMIT CHAURASIA**[1], (Member, IEEE), **AND CHIRANJI LAL CHOWDHARY**[3]

[1]Department of Computer and Communication Engineering, Manipal University Jaipur, Jaipur, Rajasthan 303007, India
[2]Department of Information Systems, College of Computer and Information Science, Princess Nourah bint Abdulrahman University, Riyadh 11671, Saudi Arabia
[3]School of Computer Science Engineering and Information Systems, Vellore Institute of Technology, Vellore, Tamil Nadu 632014, India

Corresponding author: Chiranji Lal Chowdhary (chiranji.lal@vit.ac.in)

ABSTRACT Object formation is imperative to the recent computer vision, pattern recognition, healthcare, and automation applications. The objects are generated from images by defining edges and the segmentation process. This article introduced a novel method, Outer Totality Cellular Automata (OTCA), for defining actual and continuous edges of the image objects. The OTCA analysis nearby 25 neighbourhood pixels of all the pixels and generate a unique and efficient threshold. The proposed method has three primary functions, i.e. vitality, rule mapping, and improved morphological functions. The key objectives are image smoothing, neighbourhood analysis, defining game of life rule, and edges smoothing. Notably, the proposed method aimed to segment different coloured images, i.e., RGB, HSV, and YUV. The proposed method also aimed to produce more truthful results on blurred, reflected, shaded night vision images. The experimental process demonstrates using standard open-source datasets and validated using image quality assessment parameters, i.e., entropy, PSNR, SSIM, and MSE. The results claim $3\% - 12\%$ more structural analogous, factual, and accurate than existing classical methods and recent searches.

INDEX TERMS Coloured image, edges detection, cellular automata, thresholding, vitality function, transition rule.

I. INTRODUCTION

In the recent era, coloured images have played a focal role in the fields of computer vision, pattern recognition, mixed reality, healthcare, and automation. Generally, all these fields analyse images at various levels and extract different types of image features. Edges extraction is the key feature of the image properties, and locating true and continuous edges is always challenging for researchers.

The colour space is a model used to visualize the data using different types of colours. Images, Graphs, videos, charts etc., are the most common multimedia of the colour model. Generally, a few colours make multimedia files, and the colours are generated by the specific colours used by the model. The colour model is categorized as follows: RGB, HSV, YUV, CMKY, CIE colour space etc. [1], [2], [3].

- The files generated by RGB model use either of three colours red (255, 0, 0), green (0, 255, 0), or blue (0, 0, 255) colour [1].
- The HSV model files use either Hue, Saturation, or value components and six colours: red, green, blue, cyan, magenta, and yellow [2].
- The YUV model files colour is the combination of three components: Y component represents luminance or brightness, and U and V components represent the combination of colours [2].

The associate editor coordinating the review of this manuscript and approving it for publication was Joewono Widjaja.

- The CMKY model files colour is the combination of four components: the 'C' component represents "Cyan" colour, the 'M' component represents "Magenta" colour, the 'Y' component represents "Yellow" colour, and the 'K' component represents "Key (Black)" colour [3].
- The CIE colour space combines three colours: nearly red, green, and blue. The CIE colour space is used to visualize the image in 3D space [3].

The object refers to an area surrounded by several edges. The objects are constructed by detecting all the possible edges from the multimedia file [4]. Usually, an edge is a line or boundary which may exist at the outlier of the objects. An edge may have existed where brightness changes and discontinuities of pixels intensity occurred [5]. A multimedia file may contain different shapes of edges, i.e., step, line, pulse, stairs, junction edges etc., as shown in Figure 1 [6]. The identical objects could be located by detecting true and continuous edges.

Object extraction aims to recognize an object's accurate position and shape in the multimedia file, which helps computer vision applications improve their capability. Object extraction has many computer vision applications in various fields like science, engineering, and medicine. Relevant to these fields, much work has been done in object extraction, but still, a scope has remained. For example, how to justify that the object detection model is robust and reliable? How it be guaranteed that the model recognizes truthful objects from the multimedia files caused by interference? Fortuitously, the Cellular Automata (CA) enable object detection models to be more reliable and robust. Generally, the object detection models map the objects by detecting the edges of the objects, and the edges are determined by analyzing nearby neighbourhoods.
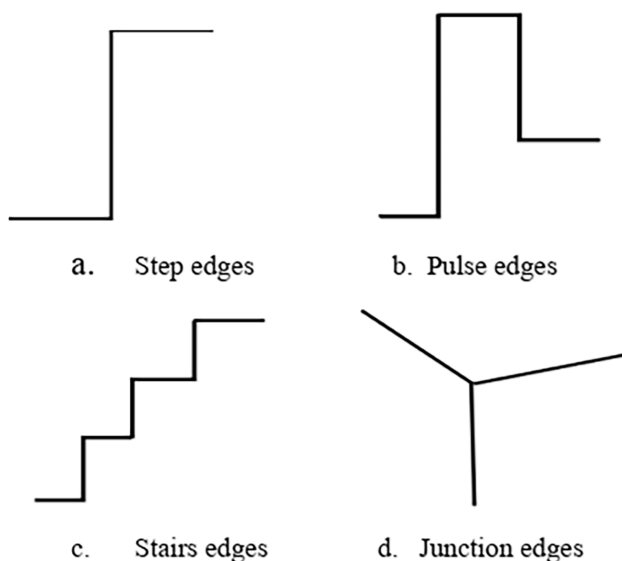

FIGURE 1. Different types of edges.

The CA provide flexibility to the object detection models to include the maximum number of neighbourhoods, which may help them to improve their robustness. Cellular Automata works behind Von Neumann's and Moore's theories [7]. The Von Neumann method works on 4-neighbourhood cells, i.e., left, right, upper, down, and itself. The Moore method works on 8-neighbourhood cells and 24-neighbourhood cells, as shown in the Figure 2. The red shaded cell represents the centred cell, and the green shaded cells represent neighbourhoods. The 25-neighbourhood method of Moore is known as the extended Moore method that includes outer and centred cells [7]. The CA work on all outer neighbourhoods and the central cell to provide robustness to the object detection models.
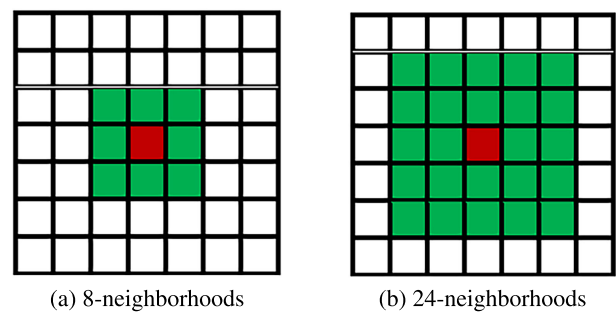

(a) 8-neighborhoods   (b) 24-neighborhoods

FIGURE 2. Moore's neighbourhood structures.

A. KEY CONTRIBUTIONS

The key involvement of the proposed article can be briefed as follows:

- Invent a CA-based new method OTCA, which focuses on different types of multimedia files for object detection.
- We focused on determining true and continuous edges from night vision, reflected noisy and noise-free coloured images. The focused edges help us to locate a truthful object.
- The results will be validated using quality assessment parameters, i.e., MSE, PSNR, SSIM, and Entropy.
- The results will be compared with classical methods, i.e., Sobel, Prewitt, Robert, and Laplacian and recent research, i.e., Mittal et al. [8]. And Mega et al. [9].

B. QUALITY ASSESSMENT

Usually, image quality parameters are used to assess the processed image. Many parameters exist to assess the quality of an image, but this section briefs only the parameters which will be used to assess the results of this article. The Mean Squared Error (MSE) quality assessment parameter finds the average difference between the source and processed image. The Mean Squared Error value is calculated using equation 1, where M and N are the size of images, $X_{i,j}$ is the current cell value of the source image X and $X'_{i,j}$ is the cell value of processed image X'. Lower MSE value states that the

TABLE 1. Comparison of different approaches.

Existing Technologies	Benchmark	Pros	Cons
Classical methods (Sobel, Prewitt, and Robert)	• First order derivation. • Gradient operator.	• Detect edges with directions. • Fast in processing.	• Produce false edges. • Susceptible to noise.
Classical methods (Canny, Laplacian)	• Second order derivation. • Gaussian operator.	• Detect true edges. • Correctly locate edges of image objects. • Low error rate.	• Susceptible to corners of objects. • Susceptible for curve shape objects. • Time consuming
Thresholding based methods	• Histogram • Clustering • Entropy • Spatial • K-means	• Locate correct location of edges. • Find accurate edges.	• Susceptible to high noise • Clustering and k-mean may suffer from continuity of edges. • Suffer from false positive or negative for small objects.
Thresholding based method (Otsu, Kittler-Illingworth)	• Histogram • Clustering	• Produce true and continues edges. • Less error rates. • Perfectly identifies edges of curved shapes.	• Susceptible to high noise • Perform badly on small objects.
Gradient based methods	• First order derivation • Kirsch compass operator • Robinson operator	• Produce strong (thin and continuous) edges. • Noise suppression. • Effectively works on curved shaped objects.	• Time consuming • Low positioning accuracy
Wavelet based methods	• Sinusoidal waves • Discrete wavelet • Haar wavelet • Watershed • Symlet	• Produce continuous edges. • Fast response. • Less error rates.	• Sampling issues. • Produce thick edges.
Hough transform based methods	• Phase stretch transform. • Gabor transforms. • Fast Fourier Transform.	• Stronger response for noisy image • Preserve originality of image	• Produce redundant features. • Time consuming.

processed image has fewer errors [10], [11].

$$MSE = \frac{1}{MN} \sum_{i=1}^{M} \sum_{j=1}^{N} (X_{i,j} - X'_{i,j})^2 \qquad (1)$$

The Peak Signal Noise Ratio (PSNR) parameter finds the ratio of original and processed image [10]. Higher PSNR value state that the quality of the processed image is high. The PSNR value of an image should be calculated using the equation 2.

$$PSNR = 10 \log_{10} \frac{(2^n - 1)^2}{MSE} \qquad (2)$$

where n is the number of bits required to represent a pixel in the image [10], [12]. For example, if a pixel uses 8 number of bits to represent a pixel then the PSNR will be as equation 3.

$$PSNR = 10 \log_{10} \frac{255^2}{MSE} \qquad (3)$$

The Structural Similarity Index Measure (SSIM) parameter measures the similarity between the original and processed image. The higher value of SSIM represents a high similarity between the images. This parameter finds the similarity by analysing Human Visual System (HVS) characteristics: loss of correlation, Luminance Distortion and Contrast Distortion [12]. The SSIM value is calculated for two images, S and G, by multiplying all three characteristics as represented in equation 4.

$$SSIM = \frac{2\mu_S \mu_G + c_1}{\mu_S^2 + \mu_G^2 + c_1} * \frac{2\sigma_S \sigma_G + c_2}{\sigma_S^2 + \sigma_G^2 + c_2} * \frac{\sigma_{S,G} + c_3}{\sigma_S \sigma_G + c_3} \qquad (4)$$

Here, μ_S and μ_G are the mean values and σ_S and σ_S are the standard deviation values of the images S and G. σ_S, G is the co-variance of the respective images and c_1, c_2, c_3 are the positive constant values used to avoid dividing by zero exception. The value of SSIM should be more significant

from 1 to 40 dB [13].

$$E = \sum P_i \log P_i \qquad (5)$$

The entropy of the image is defined by the amount of information maintained by image pixels. The higher value of entropy depicts that the pixel maintains maximum information [12]. Equation 5 is used to calculate the entropy of image pixel P.

II. RELATED WORK

This section reviews existing research related to the object detection, edge detection, image enhancement, and image segmentation. The classical methods for image segmentation play an interesting role in the recent research relevant to the image applications. In the recent research numerous methods have been introduced based on the threshold, gradient, wavelet, and Hough transform techniques.

A. CLASSICAL METHODS

The classical methods for image processing are used for edge-detection. Primarily, the classical techniques are based on first-order or second-order derivations: gradient technology and Laplacian technology. The first order or gradient-based technique discovers the edges by examination minimum and the maximum first derivative of the image. Classical techniques like Robert, Sobel, Prewitt and Canny are based on gradient technology. The second order or Laplacian-based technique finds image edges by searching zero crossings.

1) Sobel Method: This method filters the edges using a convolution operator. The operator used in this method is a 3×3 matrix, which defines the gradient operators for the x-axis and y-axis. Table 2(a) depicts a common structure of convolution operator for image regions, and Tables 2(b), and 2(c) depicts x-axis and y-axis gradient operators. Equations 6, and 7 are used to define x-axis and y-axis gradient operators (F_x and F_y) for the convolution operations. Here P_0, P_1, P_2, P_3, P_4, P_5, P_6, and P_7 are the neighbourhood pixels of the pixel $P_{i,j}$.

$$F_x = (P_2 + 2P_3 + P_4) - (P_0 + 2P_7 + P_6) \qquad (6)$$
$$F_y = (P_0 + 2P_1 + P_2) - (P_4 + 2P_5 + P_6) \qquad (7)$$

TABLE 2. a. Sobel convolution operator b. x-axis gradient operator c.y-axis gradient operator.

P_0	P_1	P_2		-1	0	1		-1	-2	-1
P_7	$P_{i,j}$	P_3		-2	0	2		0	0	0
P_6	P_5	P_4		-1	0	1		1	2	1
(a)				(b)				(c)		

2) Robert Method: This method divides the image into 2×2 size of regions and select same size of the convolution operator for x-axis and y-axis direction. The operator separately applied on each region and combined the results of all the regions to produce the target result. Due to the divide and conquer approach, the Robert method is comparatively fast and produces accurate edges. Table 3 depicts the gradient operators used for x-axis and y-axis respectively [8], [9].

TABLE 3. Robert convolution operator.

1	0		0	1
0	-1		-1	0
(a)			(b)	

3) Prewitt Method: The Prewitt technique is too like the Sobel with the only difference in size of the operator. The convolution operator of Prewitt is the size of 3×3 and its x-axis orientation is generated by rotating the y-axis orientation to 90°, and vice-versa. Table 4 depicts the x-axis and y-axis convolution operator respectively [8], [9].

TABLE 4. Prewitt convolution operator.

-1	0	1		1	1	1
-1	0	1		0	0	0
-1	0	1		-1	-1	-1
(a)				(b)		

4) Marrs-Hilderth Method:
The Marrs-Hilderth or Laplacian is a second derivation-based technique for detecting image edges. The process of the method is simpler but suffer from two big issues: generates false edges, and discontinuity of edges [8], [9]. This technique has three main steps:

Step a: Read an image and apply a low pass Gaussian filter for smoothing the image.

Step b: Enhanced the image by applying the Laplacian approach. This step applies the Laplacian method on each pixel to remove existing noise.

Step c: Apply zero crossing second derivation method for finding all possible edges.

The low pass filter of Marrs method follow the equations 8, 9 and 10 to eliminate noise effect. Here, G is the Gaussian filter of the $2 - D$ surface, and is represented in equation 8. The Gaussian filter may be varied as per the surface points (i, j), and variance (σ) between consecutive points. Equation 8

represent convolution operation ($\circledast$) between Laplacian (∇^2) of source image (F) and Gaussian Filter (G). The Laplacian of Gaussian is defined using equation 10.

$$G(i,j) = \exp^{-\frac{i^2+j^2}{2\sigma^2}} \tag{8}$$

$$H(i,j) = \nabla^2 \left[G(i,j) \circledast F(i,j) \right]$$
$$= \nabla^2 G(i,j) \circledast \nabla^2 F(i,j) \tag{9}$$

$$\nabla^2 G(i,j) = \left(\frac{i^2+j-2\sigma^2}{\sigma^4} \right)^{-\frac{i^2+j}{2\sigma^2}} \tag{10}$$

B. THRESHOLDING BASED METHODS

Thresholding is the easiest technique for image processing, in which a common value is used to process pixels of the image. The common value is known as the threshold value, which is estimated by analyzing pixels intensity. The threshold value is a global value, which means using a single value or a range of values for all the pixels, and it has different values according to the regions of the image. The region-based threshold value is known as local thresholding or adaptive thresholding. After finalizing the threshold value, it should be compared with image pixels and decide the binarization of the image [14]. Sharma et al. suggest image segmentation and transformation method in their research using outer cellular automata. A range of threshold value has been generated by analysing nearby neighbourhood pixels of the image. The proposed method may include number of neighbourhoods at different radius level to generate a robust threshold and is applied to work on any type of color images [15], [16].

Xu et al. presented a paper for the detection of image patterns by dividing the images into tiles. The proposed research identifies image mosaics by finding the edges of the image tiles. The edges of the tiles are found by calculating the mean-value of associated pixels. The proposed method finds the image mosaics by maintaining 80% of image originality [17]. Hussain et al. introduced a histogram-based technique which is used to improve the quality of dark images. This paper divides the image into local regions by histogram technique and generates one aggregate value for enhancing the image pixels [18]. Mittal et al. presented a method, B-Edge, for the detection of image edges by mapping multiple threshold values with the help of neighbourhood pixels. In this paper, produced results are compared with existing classical techniques [8]. Mega et al. presented a paper for comparing the results of classical methods for HSV and YUV colour images [9]. Cao et al. presented a paper for parallel image edge detection algorithm using improved *Otsu-Canny method* for the Hadoop platform. The proposed method smoothed the source images using the Gaussian operator by dividing gradients into clockwise and anti-clockwise directions [19]. Wu et al. invented a novel method *BFAN* for object detection using featured aggregation network [20]. Usmani et al. introduced the video object segmentation approach by defining the correlation between video frames [21]. He et al. presented a survey paper for finding defective products. This paper reviewed a few research on computer vision, image segmentation and deep learning, which are used for finding defective products [22].

C. GRADIENT BASED METHODS

Image gradients are characterized by the derivation of the image and the derivation is defined by the changes in the intensity level of image pixels. The derivation approach detects the edges of the image by locating pixels at minimum and maximum point. The maximum and minimum point is located by adjusting origin, generally, the origin should be a centre point or zero. There are two types of approaches for edge formation based on derivation, namely: first-order and second-order. The first-order derivation approach works by looking at minimum and maximum and second-order derivation works by crossing zero. The gradient-based methods i.e., Kirsch Compass and Robinson operator show very stimulating results in the field of image processing [23], [24], and [25]. Wu et al. proposed a morphological gradient-based color image segmentation method. The opening and closing operations are used in this article for thinning or thickening the image edges. The proposed method has experimented on different types of color images and claimed 10% more efficient results and about 1% more accuracy and recall [26].

Li et al. presented a method for image edge detection based on Gaussian Kernel. This method finds the weak pixels of the image and applies the ESM algorithm to smooth these pixels [27]. Zheng et al. introduced a super-resolution method for edge detection and enhancement of MRI images [28]. Huang et al. presented a paper for image smoothing using diffusing technology with gradient. This paper introduced two models, which are used to extract image objects and de-noising the image by retaining texture information and edges of the objects [29]. Fang et al. presented a paper for scale and gradient-based methods for image smoothing by removing high and low contrasting text pixels and retaining sharp and fine boundary pixels. This method fixes a scaling value for deciding the high quality of the image edges [30]. Wang et al. presented a paper for the assessment of visual quality for the screen content images. The proposed model of this paper has formed an efficient full-reference quality assessment technique, in which edges are formed by extracting gradient-domain for better visual representation [31]. Kabir et al. presented a method for image edge detection based on gradient intensity. In this method, the edges of image objects are detected by analyzing the horizontal and vertical neighbourhood intensity of pixels, and the boundary edges are detected with the help of derivation slopes, which exist between consecutive pixels [32]. Yahya et al. introduced two types of filters for image edge detection and enhancement based on diffusion and variance. The diffusion filter uses a non-linear gradient magnitude technique to remove noise from the image. The variance filter is implemented using the first and second-order derivation approach, which helps in finding edges from the image [33].

D. WAVELET BASED METHODS

Wavelet is an oscillation with an initial amplitude of zero, and it may change in an upward and downward movement and return to the initial level. This type of transformation has been implemented in the various domains of image-based technologies. The well-known of such types of technologies are Discrete Transformation (Cosine and Sine), Haar Wavelet, Watershed, and SymLet [34], [35]. Formally, the wavelet transform is demarcated as a mathematical model to analyse an identifiable pixel of the image. However, the wavelet transforms found its essence and originated from many computer vision study domains. Tzu Ching Wu et al. invented a new model for identification of abnormal tissues and organs from medical images. A Wavelet Transformation technique has been implemented with the model without using any filter. The authors claimed a robust segmentation of images with high PSNR [36]. Yang et al. used Haar Wavelet Transformation in their research for breast cancer detection. A multiclass U-net based approach introduced to efficiently segment the MRI images. The authors shown 87.48% accuracy in their results for identification of breast cancer [37].

Shi et al. presented a wavelet-based method for finding edges from the noisy image and heterogeneous environment. In order to achieve this objective, the proposed method combines concepts of two polarimetric and weighted gradients. The polarimetric method helps to find a weak and strong edge, while the weighted gradient method process an image which has heterogeneous features [38]. Chengtao et al. presented a paper for the implementation of a trilateral filter for image edge enhancement. The proposed research also employed a kernel-based algorithm to extract image edges by analyzing nearby pixels [39]. Jiang et al. presented a method for developing a channel for image object recognition and enhancements. In this paper, an improved canny algorithm is used by adjusting parameters for object recognition and a median filter is used to enhance recognized objects [40]. Liu et al. super-resolution reconstruction model. In this paper, approximately 20 convolution filters are applied to the image at various layers to smooth the image and apply the LoG algorithm for image edge formation [41]. Shen et al. presented a method including the canny method and watershed method for image edge detection and segmentation by dividing the image into 5×5 clusters [42]. Tian et al. introduced an adaptive model for image enhancement by masking operators. In this method, the model is designed by studying the roughness of a surface. The roughness detection method is a non-linear approach which analysis the surface by imaging technology and de-noises the image pixels. The pixel de-noising is performed by a masking operator, which amplifies the image pixels [43]. Sabir et al. present a segmented-based image defogging method for image enhancement by adjusting the pixel's colour, contrast, and visibility. The proposed research's defogging method is

analyzing the images dark and light channels and designing a filter with the help of channels [44].

Algorithm 1 Algorithm for Vitality and Luminosity Function

1: **procedure** Vitality(*Image S*, *int M*, *int N*)
2:    $cop[3], [3] = \{(\frac{1}{9}, \frac{1}{9}, \frac{1}{9}), (\frac{1}{9}, \frac{1}{9}, \frac{1}{9}), (\frac{1}{9}, \frac{1}{9}, \frac{1}{9})\}$
3:    **for** $i \leftarrow 0$ to $M - 1$ && $j \leftarrow 0$ to $N - 1$ **do**
4:      $k = 0$
5:      $l = 0$
6:      **for** $k < 3$ && $l < 3$ **do**
7:        $V[k][l] = S[i][j]$
8:        $k + +$
9:        $l + +$
10:        $G[0], [0] = V[0], [0]$
11:        $G[0], [4] = V[0], [2]$
12:        $G[4], [0] = V[2], [0]$
13:        $G[4], [4] = V[2], [2]$
14:      **end for**
15:      **for** $i \leftarrow 0$ to 2 **do**
16:        $G[0][i] = V[0][i]$
17:        $G[i][0] = V[i][0]$
18:        $G[4][i + 1] = V[2][i]$
19:        $G[i + 1][4] = V[i][2]$
20:      **end for**
21:      **for** $k \leftarrow 1$ to 3 && $l \leftarrow 1$ to 3 **do**
22:        $V[k - 1][l - 1] = G[k][l] \circledast cop[k - 1][l - 1]$
23:        $i = i + 3$
24:        $j = j + 3$
25:      **end for**
26:    **end for**
27: **end procedure**
28: **procedure** Luminosity(*Image S*, *int M*, *int N*)
29:    **for** $i \leftarrow 0$ to $M - 1$ && $j \leftarrow 0$ to $N - 1$ **do**
30:      $G[i][j] = S[0, 0, 255] * 0.3 + S[0, 0, 255] * 0.59$
                   $+ S[0, 0, 255] * 0.11$
31:      $S = G$
32:    **end for**
33: **end procedure**

E. HOUGH TRANSFORM BASED METHODS

In digital image processing, Hough transform plays an important role that works by extracting image features. This technique helps to identify objects from an image by locating the edges of line and circle shapes. The Hough transform method maps a function that transforms an image's pixels into a line or curve. The information needed to draw these lines will be provided by detecting and identifying some groups of pixels that share common characteristics, such as being on the same line or intersecting a set of lines, utilizing some Hough space features [45], [46]. In recent years, Hough transform-based methods i.e., Phase Stretch, Gabor, and Fast Fourier-related research have been encountered and shown very stimulating results.
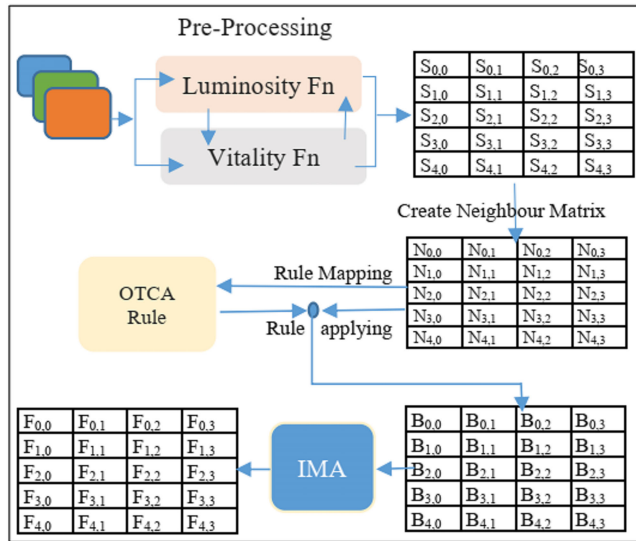
FIGURE 3. Proposed OTCA methodology.

Phase Stretch Transform (PST) is a non-linear and phase manipulation frequency-based process used to extract image features. Edges formation from noisy images is a key objective of phase stretch transformation. The PST produces the binary image with 0 or 1 values whose size is the same as the original image. PST is also able to enhance the produced binary image by manipulating high-frequency components. Generally, PST produces robust results for noisy and low-contrast images but is comparatively computationally complex [47]. Xu et al. proposed an anisotropic PST algorithm for the separation of initiated slop phase-disparity minuscule images. The authors have improved the results of traditional PST by 30% and claim robust results as compared to classical image segmentation methods. The results of the research were validated using consistency error and rand index [48]. He et al. have combined anchored regression with traditional PST to extract all the local features from noisy medical images. The authors claimed faster results with low latency and improved PSNR as compared to the traditional methods [49]. Overall, the PST is a useful technique in computer vision and image processing, especially when processing noisy and intricate feature images. It is helpful in a variety of applications where feature extraction and pattern recognition are essential since it can sharpen edges and highlight features.

Gabor Transform is a computational method for pattern identification and image analysis. The Gabor Transform is a significant tool in many applications, including texture analysis and image processing, because it is especially effective for examining and describing both the time and frequency aspects of signals. Generally, the Gabor transform is a linear filter that works by combining the time and frequency domain of Fourier and enhancing the image quality using Gaussian filters. Gabor transforms play intelligently with digital images for locating robust textures and objects [50], [51]. Virodhi Dakshayani et al. suggest an

image-denoising and edges extraction model using Gabor Transforms. The authors have measured the performance using SSIM, PSNR, and MSE parameters and compared it with classical methods. The research claimed high PSNR and low MSE comparatively [52]. Gao et al. proposed a two-dimensional-based pattern recognition method. This study extracts image features by affecting color, shape, and textures. The test results of the study claimed that the image is processed effectively and accurately [53]. Venkatachalam et al. discussed an innovative approach using Gabor filtering and Walsh-Hadamard transforms. The aim of the study is to segment the medical images and retrieve all the properties of the image. This study used the Fuzzy C-mean method to define the similarity between segmented and original images. The results of the study claimed that the method provides all the possible features of the medical image in less time as compared to other Hough transform techniques [54]. Ullah et al. presented a survey on object tracking systems and introduced an IoT-based method for tracking wildfire, deadly vapor, and bio-synthetic mixtures objects on wireless networks [55]. Overall, the Gabor Transform is an adaptable apparatus for processing images with difficult features and textures.

Fast Fourier Transform (FFT) is a widely used technique for pattern recognition, image enhancement, and compression. Generally, FFT uses low-pass and high-pass filters to enhance the images, frequency domain information for pattern recognition, and Discrete Cosine Transformation for image compression. FFT is computationally complex and not perform accurately with noisy images [56]. Zak et al. suggest a convolution and FFT-based method for image classification. In this research, convolution operator is used to filter the image features for classification and Fourier Transform helps to speed up the performance of method [57].

Wu et al. presented a paper based on Hough transform for finding zebra crossing by determining road image edges. The zebra crossing edges are formed by finding straight and parallel lines, where thresholding concepts remove the shadow effects [58]. Meng et al. presented a paper for water land image segmentations based on wavelet transformation. The source images are smoothed by applying various filters, i.e., Gaussian, Gabor, and Wavelet. The image segmentation is performed by dividing the image into four channels according to pixels frequency and selecting best-suited features for finding edges of the segment [59]. Hu et al. presented a method for image editing and correction using a wavelet transformation approach. The image editing process is performed by finding the edges of image objects and texture. The non-gaussian features of the object are presented in [60]. Table 1 summarises existing research with used technology, methods and their achievements and limitations.

III. PROPOSED OTCA METHOD
A. OVERVIEW
The proposed methodology has five functions to obtain the objectives. The proposed method accept noisy or noise
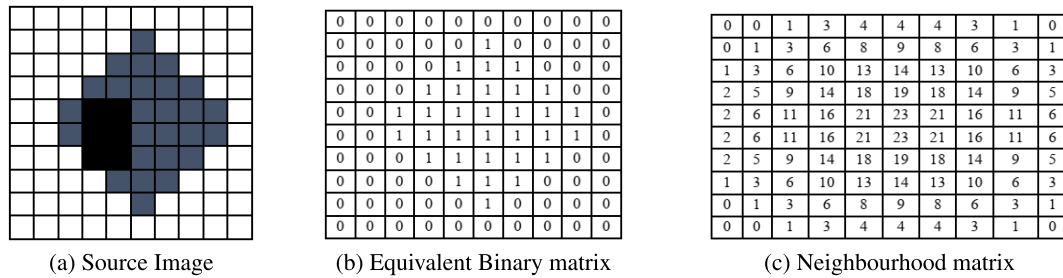
| (a) Source Image | (b) Equivalent Binary matrix | (c) Neighbourhood matrix |

FIGURE 4. Neighborhood-matrix generation.

Algorithm 2 Algorithm for OTCA Rule Mapping and Edge Plotting

1: $S_{M,N} = Source\ Image$
2: $N_{M,N} = Neighbourhood\ matrix$
3: $B_{M,N} = \{0\}$
4: $Set\ S_1 = 0, S_2 = 0, Even = 0, Odd = 0$
5: $m = Min(N_{M,N})$
6: $n = Max(N_{M,N})$
7: **for** $i \leftarrow m$ to n **do**
8:     **if** $i\%2 == 0$ **then**
9:         $S_1 = S_1 + i$
10:         $Even + +$
11:     **else**
12:         $S_2 = S_2 + i$
13:         $Odd + +$
14:     **end if**
15: **end for**
16: $T_1 = \left\lfloor \frac{S_1}{Even+1} \right\rfloor$
17: $T_2 = \left\lfloor \frac{S_2}{Odd-1} \right\rfloor$
18: **for** $i \leftarrow 0$ to $M - 1$ && $j \leftarrow 0$ to $N - 1$ **do**
19:     **if** $((N[i][j] \geq T_1 \&\& N[i][j] \leq T_2)$ && $S[i][j]) \neq 0$ **then**
20:         $B[i][j] = 1$
21:     **else if** $((N[i][j] \geq T_1 \&\& N[i][j] \leq T_2)\ \|\ S[i][j]) == 0$ **then**
22:         $B[i][j] = 0$
23:     **end if**
24:     **for** $x \leftarrow i - 1$ to $i + 1$ && $y \leftarrow j - 1$ to $j + 1$ **do**
25:         **if** $S[i][j] \neq 0$ && $N[i][j] < T_1$ **then**
26:             $B[i][j] = 1$
27:         **end if**
28:     **end for**
29: **end for**

---

free image of any colour for object identification. The first function, "pre-processing" has two methods vitality and luminosity for smoothing and colour conversion. The second function, "Neighbourhood-Matrix Generation" is used to analyse nearby neighbours of the image pixels and generate a neighbourhood matrix. The third function "OTCA rule mapping" which is used to map a rule used for processing the image pixels. The fourth function is "Edge plotting", which is used to apply mapped rule on the neighbourhood matrix to identify edges of the image objects. The fifth function is "Edges enhancement", which is used to improve the quality of the object edges.

As discussed in the Section I, the CA technology analysis near neighbourhood pixels of images or frames of video at various levels. The processed or current pixel of a source image is to be considered a zero-level pixel, and the outer pixels of the current pixel are to be considered first-level pixels. So generally, the CA processes input data using a function known as the transition function. The transition function is a rule or method, which takes the pixel of an image as the current state, processes the current state, and produces a new pixel as the new state. To generate a robust function, the proposed OTCA (Outer Totality Cellular Automata) method presented in Figure 3 analyse the outer pixels of the image pixel's. The more number of pixels provide robustness to the system and helps to improve accuracy.

1) Pre-processing: This step of the proposed methodology has two primary functions, i.e., vitality function and Luminosity function. The vitality improves the quality of the source image, and the luminosity function converts the coloured image into a grey image. The vitality function operates using the principles of low pass filter, where each associated cell's average intensity is determined and any nearby pixels with intensities below the average are changed to the corresponding averaged intensity value. The vital function divide the
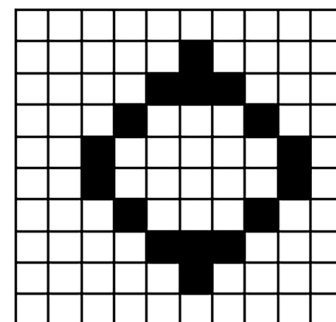

FIGURE 5. Edges plotted for image object.

Algorithm 3 Algorithm for Improved Morphology

1: Read input $C_{M,N}$
2: Initialize structuring element SE of Size 3×3
3: $SE = [[0, 0, 0], [a, 1, a], [1, 1, 1]]$
4: $B_{M,N} = \{0\}$ ▷ Value of a is either 0 or 1
5: Origin $SE[1], [1]$
6: Set $PR[][] = \{0\}$
7: **for** $i \leftarrow 0$ to $M - 1$ && $j \leftarrow 0$ to $N - 1$ **do**
8:      $count = 0$
9:      **if** $c[i][j] == origin$ **then**
10:          **for** $x \leftarrow i - 1$ to $i + 1$ && $p \leftarrow 0$ to 3 **do**
11:              **for** $y \leftarrow j - 1$ to $j + 1$ && $q \leftarrow 0$ to 3 **do**
12:                  **if** $c[x][y] == SE[p][q]$ **then**
13:                      count++
14:                  **end if**
15:              **end for**
16:          **end for**
17:      **end if**
18:      **if** $count == 9$ **then**
19:          $PR[i][j] = 1$
20:      **end if**
21: **end for**
     $T = SE[0], [0] = SE[1], [0] = SE[2], [0]$
22:    $= SE[2], [1] = SE[2], [2] = SE[1], [2]$ ▷ Rotate SE
     $= SE[0], [2] = SE[0], [1] = T$

0	0	0	0	0	0	0	0	0	0
0	0	0	0	0	1	0	0	0	0
0	0	0	0	1	1	1	0	0	0
0	0	0	1	0	0	0	1	0	0
0	0	1	0	0	0	0	0	1	0
0	0	1	0	0	0	0	0	1	0
0	0	0	1	0	0	0	1	0	0
0	0	0	0	1	1	1	0	0	0
0	0	0	0	0	1	0	0	0	0
0	0	0	0	0	0	0	0	0	0

FIGURE 6. Result of edge plotting step.

FIGURE 7. Enhanced edges produced by IMA.

source image $S[M, N]$ into the regions of 3×3 and apply the same size of average operator on each region to smooth them. The luminosity function extract all the colour components from source image $S[M, N]$ and combine them in the ratio of 30%, 59%, and 11% [15]. The Algorithm 1 depicts the working of vitality and luminosity functions with running time is $O(MN)$

2) Neighbourhood-Matrix Generation: This step counts the live neighbourhoods for all the pixels of the grey image produced by pre-processing step. The pixel with value 1 to consider alive and value 0 to be consider dead. The proposed OTCA method considers outer pixels up to the second level of radius (as per Figure 2 24-neighbourhoods). Equation 10 used to generate the neighbourhood matrix $N[M, N]$ of the source image $S[M, N]$. The Figure 4 shows the process of generating neighbour matrix with example. Figure 4a represent the source image, 4b represents binary image with alive and dead pixels, and 4c represent number of alive neighbourhoods.

$$N_{i,j} = \bigcup_{\substack{i=0 \\ j=0}}^{\substack{i=M-1 \\ j=N-1}} \sum_{\substack{x=i+2 \\ y=j+2}}^{\substack{x=i-2 \\ y=j-2}} S_{x,y} - S_{i,j} \quad (11)$$

3) OTCA rule mapping: The OTCA rule is decided according to the number of neighbourhoods up to second level of the processed cell. The neighbourhood matrix
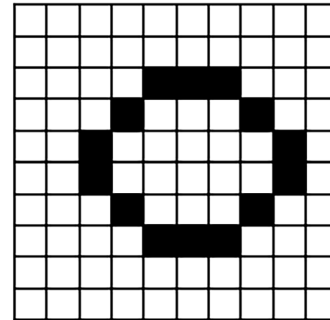
contains 26 possible values, i.e., 0 to 25. The rule is finalized by averaging all the even and odd values respectively. The sum of even and odd numbers from 0 to 25 is 156 and 169. To calculate average of sum of even numbers, the sum is divided by 14 due to one extra even level i.e., 0 to 2 as compared to odd level i.e., 1. Hence the average of even numbers is 11 (0+2+4+6+8+10+12+14+16+18+20+22+24 = 156/14) and average of odd numbers is calculated by dividing the sum by remaining 12 numbers, so average is 14 (1+3+5+7+9+11+13+15+17+19+21+23+25 = 169/12). So, finally the threshold value for the image will be 11 and 14. The threshold value vary from image to image, and this variation helps to generate robust results. Equations 12 to 17 are used to finalize threshold values for the source image $S[M, N]$, whose neighbourhood matrix is $N[M, N]$.

$$m = min\left(N_{M,N}\right) \quad (12)$$

$$n = max\left(N_{M,N}\right) \quad (13)$$

$$S_1 = \sum_{i=m}^{i=n} i \ if \ i\%2 = 2 \quad (14)$$

$$T_1 = \left\lfloor \frac{S_1}{even + 1} \right\rfloor \quad (15)$$

$$S_2 = \sum_{i=m}^{i=n} i \ if \ i\%2 \ != 2 \quad (16)$$

$$T_2 = \left\lfloor \frac{S_2}{odd - 1} \right\rfloor \quad (17)$$

4) Edge plotting: The Algorithm 2 represent process of OTCA rule mapping and edge plotting functions. The

computational complexity associated with Algorithm 2 is $O(MN)$. Once the rule or threshold function is decided, it should be applied to all the cells of the source image by following the respective neighbourhood matrix. The threshold function of the proposed method works as a global or unique function for all the cells, which read the current state from the cell of the source image and the corresponding value of the neighbour matrix and generates a new state by the following criteria:

- If a cell of the source image has a value 0, its new state remains dead or 0.
- If a cell of the source image is alive and the corresponding neighbour matrix cell has a value more than 14, it dies due to overcrowding.
- If a cell of the source image is alive and the corresponding neighbour matrix has a value less than 11, it dies due to loneliness, but if its adjacent outer cell is a living cell, it remains alive.
- If a cell of the source image is alive and the neighbour matrix has a value from 11 to 14, it goes on living. After applying the mapped rule on source image Figure4 and respective neighbourhood matrix Figure 2, the resultant temporary matrix of the edge plotting step will be as Figure 5.

The result of step 4 is in the form of a matrix containing binary values, i.e., 0 and 1. To produce a result as an image, the value 1 converts into black pixels and 0 converts into white pixels. Figure 5 shows an equivalent image of the Figure 2 i.e., edges plotted for the source image object.

5) Edges Enhancement: This step used to improve the quality of edges because the plotted edges may be blurred, double edges, and discontinuous. An Improved Morphology Algorithm (IMA) has been used to enhance the edges. The IMA algorithm read the produced image $C[M, N]$ return by Alogrithm 2. A structuring element SE of size 3×3 has been initialized and applied on $C[M, N]$ to smooth the image. The detailed process of IMA is depicted in Algorithm 3. Figure 6 shows enhanced results after applying the IMA algorithm on the result (Figure 7) produced by the edge plotting step.

IV. EXPERIMENTAL RESULTS

A. DATA SET

The proposed methodology has been experimented on approximately 1000 training and test images, which are taken from the Berkeley and Kaggle datasets. This section depicts the result of 20 images i.e., 5 are RGB, 10 are HSV and YUV, and 5 are noisy, shaded, night vision and reflected images.

B. RESULTS DISCUSSION AND EVALUATION

The proposed method is successfully tested on RGB, HSV and YUV colour space images. The tested colour images are night vision, noisy, shaded and reflected. The proposed

method results are compared with the results of classical methods, Mittal et al. [7] and Mega et al. [8]. The performance of the proposed method is validated with the help of three criteria: similarity analysis, error rate measurement, and accuracy.

TABLE 5. Image quality assessment parameters.

Parameters	Range	Acceptable Value	Whether Min/Max
Entropy	$[0, 1]$	$[0.3, 0.8]$	Max
PSNR	$[0, 100]$	$[60, 80]$	Max
MSE	$[0, 1]$	$[0.03, 0.11]$	Min
SSIM	$[-1, 1]$	$[0.6, 0.8]$	Min

TABLE 6. Average values of Entropy, PSNR, SSIM, and MSE for RGB colour images.

Validation Criteria		SSIM	MSE	PSNR	Entropy
Classical Methods	*Prewitt*	0.444493	0.147749	58.50161	0.127647
	Sobel	0.444420	0.148048	58.47404	0.128520
	Canny	0.397677	0.119180	57.45621	0.336973
M. Mittal Method		0.541983	0.108207	59.37434	0.205193
Proposed OTCA Method		0.555487	0.101640	61.24083	0.372033

1) Similarity analysis: This criterion helps to decide whether the produced edges of the image belong to the original source image or not. The similarity of the images could be analyzed with the help of quantitative and qualitative methods. The quantitative method analyzed the similarity between images using entropy, and PSNR (discussed in Section I-B). The qualitative method analyses the similarity between the images using SSIM (discussed in Section I-B). The higher value of entropy, PSNR, and SSIM expresses high similarity between source and resultant images.

2) Error rate measurement: The error rate of the resultant image decides whether the produced edges are true or false. The error rate of the image is measured using a quantitative method. The MSE (discussed in Section I-B) is used to measure the errors in the resultant images. The MSE is used to measure how much the resultant image is closer to the original

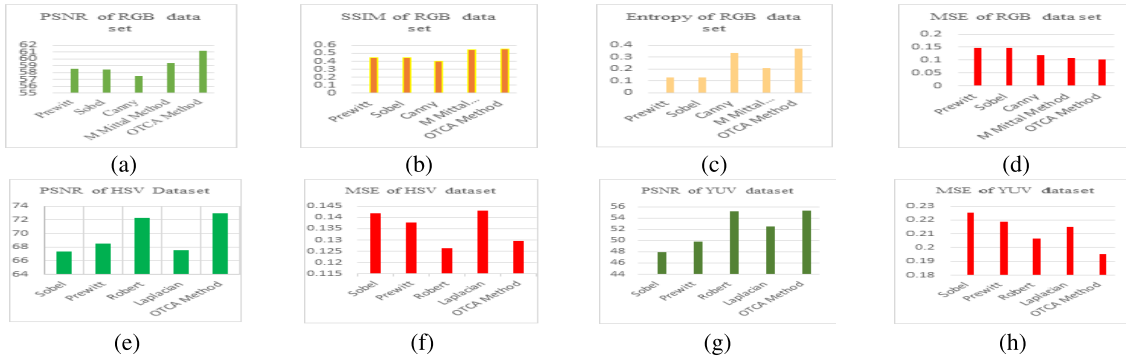**FIGURE 8.** Example of proposed methodology processes.

FIGURE 9. Comparative analysis of RGB, HSV and YUV images.

image.The smaller value of the MSE state that low error rate, closer and good correlation between resultant and original image. Table 5 depicts possible range of these parameters, accepted values, and assumption: whether the value should be minimum or maximum.

TABLE 7. Average values of PSNR, and MSE for HSV colour images.

Validation Criteria		PSNR	MSE
Classical Methods	Sobel	67.386	0.141688
	Prewitt	68.508	0.137806
	Robert	72.268	0.126474
	Laplacian	67.528	0.143003
OTCA Method		72.992	0.129644

Entropy for the image defined as amount of information retained by the pixel; maximum value express that the image contains maximum information about pixels intensity. The PSNR of an image expressed quality of resultant image in terms of noisy image. Higher value of PSNR expressed lesser error and sophisticated for noisy image. The SSIM value expressed that how the resultant image is similar with the source image. The higher value of SSIM express that the produced edges are true. The MSE of an image specify that how much the resultant

TABLE 8. Average values of PSNR, and MSE for YUV colour images.

Validation Criteria		PSNR	MSE
Classical Methods	Sobel	47.9436	0.22519
	Prewitt	49.7680	0.21864
	Robert	55.1574	0.20670
	Laplacian	52.4336	0.21504
OTCA Method		55.2652	0.19534

TABLE 9. Noisy data set results.

Noisy Data Set	Quality Assessment Parameters			
	SSIM	PSNR	MSE	Entropy
Noisy 1	0.606	59.89	0.093	0.364
Noisy 2	0.591	59.43	0.074	0.364
Noisy 3	0.626	57.34	0.120	0.684
Noisy 4	0.604	60.03	0.065	0.268
Noisy 5	0.631	65.27	0.019	0.442

image is close to the source image. Lesser value of MSE express that the produced edges are accurate.

TABLE 10. Result evaluation of proposed methodology.

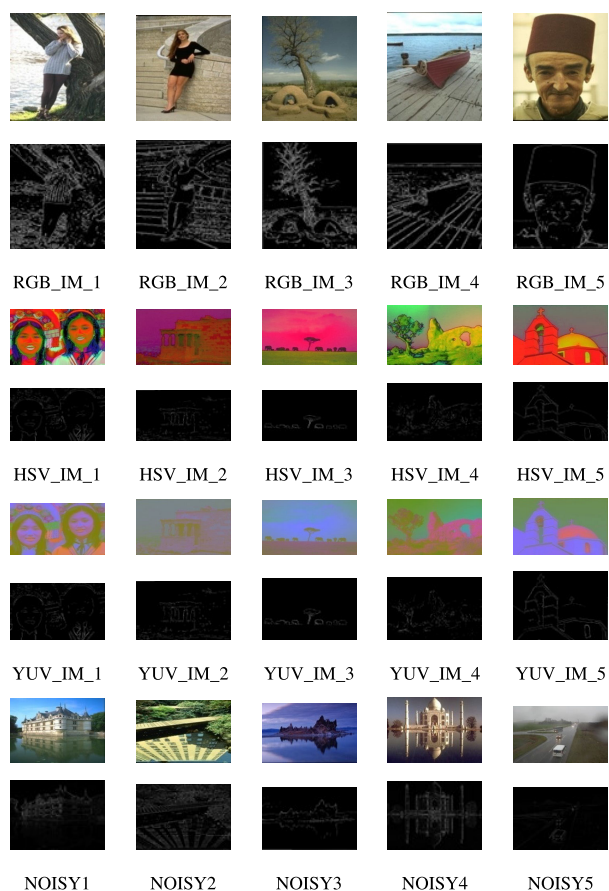| Type of Image	Average Similarity Rate	Average Error Rate	$SI \cup RI$	$SI \cap RI$	Accuracy
RGB	61.24db	0.105	99.895	100	99.89%
HSV	72.99db	0.129	99.871	100	99.87%
YUV	55.27db	0.195	99.805	100	99.80%
Noisy	60.39db	0.175	99.825	100	99.82%

FIGURE 10. Experimented results of RGB, HSV, YUV and noisy images.

As discussed in Section III the proposed methodology has primarily five steps to obtain the desired results. Figure 8 depicts the results of the entire process of the proposed methodology, which was experimented on the aeroplane image. The figure contains images of different stages i.e., source image, intermediate results i.e., Figure 8b colour conversion, Figure 8c enhanced grey image, Figure 8d neighbourhood matrix, Figure 8e plotted edges, and Figure 8f enhanced edges with respect to the objects that exist in the images.

Figure 10 shows results on selected RGB, HSV, YUV, and Noisy images. The references of RGB images are 181091, 388016, 54082, 138078, and 189080. The references of HSV and YUV images are 18035, 189003, 227040, 253036, and 317080. The references of noisy, shaded, night vision and reflected images are 102061, 148026, 143090, 288024 and 201080.

Figure 10 visualize the source and final resultant image with their reference number taken from the Kaggle dataset. The research produced a massive amount of data, and discussion among these data creates a complex analysis, so the result discussion has been performed using average values of the respective quality measurement parameters. Figure 9 shows the comparative analysis of RGB, HSV and YUV images for the difference between classical methods and existing proposed method. The PSNR, SSIM and Entropy is higher as comparison to classical methods for RGB images and the values of MSE are smaller than the classical method which signifies that the edges of resultant images are similar to the source images. Tables 6, 7, 8, and 9 show average entropy, PSNR, SSIM, MSE, and RMSE values produced by the proposed methodology and the same are compared with classical methods and recent research i.e., M Mittal et al. [8] and KW Mega et al. [9].

3) Accuracy: The accuracy of the proposed object detection model is decided using the standard image quality measurement parameters i.e., entropy, PSNR, SSIM, and MSE (discussed in Section I-B) [10], [11], [12], [13]. The higher values of entropy, PSNR, and SSIM, and lower values of MSE, and RMSE express high accuracy. The entropy, PSNR, and SSIM parameters are used to define the similarity rate, and MSE, and RMSE are used to define the error rate between the source and resultant image. The accuracy index of the produced result is determined by using the Jaccard similarity index. Equation 18 is used to define the accuracy index $JD_{SI}(SI, RI)$ between source image SI and resultant image RI. The Jaccard method defines the accuracy index using the common and combined features of the source and resultant image. Table 10 represent the

similarity rate, error rate, and accuracy of the different types of source images. The value ($SI \cup RI$) is 100, and it represent that, the 100% features of both images are exist in set. The value of $SI \cap RI$ is determined by subtracting the average error form the union of both images.

$$JD_{SI} = \frac{SI \cup RI}{SI \cap RI} \times 100 \qquad (18)$$

As per the results showing in figures and tables, the authors claim that:

- The proposed OTCA method can process different types of colour images i.e., RGB, HSV, and YUV regardless of any type of noise.
- The similarity, and error rate show the objects identified by the OTCA method are very similar to the source image with less error.
- The accuracy of the OTCA method reach up to 99.89% and maintain 99.80% as minimum accuracy.

V. CONCLUSION

Object detection plays an important role in various applications i.e., autonomous driving, healthcare systems, biometric authentication systems, and mixed reality. Object detection is the key factor of these applications, we suggest that our study is the beginning of a research stream that focuses on exact object extraction from various colour images in challenging circumstances as an extension of the in-complexity analysis of uncertainty estimates in object detectors. In this article, a cellular automaton-based method has been proposed for object extraction from different coloured images. The proposed method analysis all the image pixels and mapped a rule to comprises a global threshold. The threshold is compared with all the image pixels to locate edges of the objects. Moreover, the vitality function, and improved morphological algorithm has been applied to obtain true, thin, and continuous edges up to 99.89% accuracy. The experimented results of the proposed method have been validated using different image assessment parameters, i.e., entropy, PSNR, SSIM, and MSE. Detailed experiments on different coloured images state that the extracted edges have high entropy, PSNR, and SSIM and less MSE. Based on the results, we state that the proposed OTCA method produce efficient results for RGB, HSV and noisy image, but some improvement is required for the YUV images. Future research will enhance the thresholding by analysing more pixels to extract exact edges from the YUV-coloured images.

REFERENCES

[1] Y. Chang and N. Mukai, "Color feature based dominant color extraction," *IEEE Access*, vol. 10, pp. 93055–93061, 2022.

[2] H. Li, X. Zhao, A. Su, H. Zhang, J. Liu, and G. Gu, "Color space transformation and multi-class weighted loss for adhesive white blood cell segmentation," *IEEE Access*, vol. 8, pp. 24808–24818, 2020.

[3] N. John, A. Viswanath, S. Vishvanathan, and S. Kp, "Analysis of various color space models on effective single image super resolution," in *Intelligent Systems Technologies and Applications*, vol. 384. Kochi, India: Springer-Verlag, 2016, pp. 529–540.

[4] H. Rong, A. Ramirez-Serrano, L. Guan, and Y. Gao, "Image object extraction based on semantic detection and improved K-means algorithm," *IEEE Access*, vol. 8, pp. 171129–171139, 2020.

[5] S. K. Sharma, C. Lamba, and V. Rathore, "Otca approach towards blurred image feature estimation and enrichment," in *Information and Communication Technology*. Berlin, Germany: Springer, 2018, pp. 329–338.

[6] S. K. Sharma, C. S. Lamba, and V. S. Rathore, "Radius based cellular automata approach for image processing applications," in *Proc. 8th Int. Conf. Comput., Commun. Netw. Technol. (ICCCNT)*, Jul. 2017, pp. 1–5.

[7] A. Kumar and S. K. Sharma, "Information cryptography using cellular automata and digital image processing," *J. Discrete Math. Sci. Cryptogr.*, vol. 25, no. 4, pp. 1105–1111, May 2022.

[8] M. Mittal, A. Verma, I. Kaur, B. Kaur, M. Sharma, L. M. Goyal, S. Roy, and T.-H. Kim, "An efficient edge detection approach to provide better edge connectivity for image analysis," *IEEE Access*, vol. 7, pp. 33240–33255, 2019.

[9] K. W. Mega, X. Yu, and J. Li, "Comparative analysis of color edge detection for image segmentation," in *Proc. Int. Conf. Comput. Pattern Recognit.*, New York, NY, USA, Jun. 2018, pp. 93–101, doi: 10.1145/3232829.3232845.

[10] U. A. Bhatti, Z. Ming-Quan, H. Qing-Song, S. Ali, A. Hussain, Y. Yuhuan, Z. Yu, L. Yuan, and S. A. Nawaz, "Advanced color edge detection using Clifford algebra in satellite images," *IEEE Photon. J.*, vol. 13, no. 2, pp. 1–20, Apr. 2021.

[11] P. Ji, J. Feng, F. Ma, X. Wang, and C. Li, "Fingertip detection algorithm based on maximum discrimination HOG feature in complex background," *IEEE Access*, vol. 11, pp. 3160–3173, 2023.

[12] P. Upadhyay and J. K. Chhabra, "Multilevel thresholding based image segmentation using new multistage hybrid optimization algorithm," *J. Ambient Intell. Humanized Comput.*, vol. 12, no. 1, pp. 1081–1098, Jan. 2021.

[13] C. Wang, J. Yang, and H. Lv, "Otsu multi-threshold image segmentation algorithm based on improved particle swarm optimization," in *Proc. IEEE 2nd Int. Conf. Inf. Commun. Signal Process. (ICICSP)*, Sep. 2019, pp. 440–443.

[14] S. K. Sharma, A. Kumar, and U. P. Singh, "Enhanced edges detection from different color space," in *Proc. 4th Int. Conf. Inf. Manag. Mach. Intell.*, New York, NY, USA, Dec. 2022, pp. 1–6, doi: 10.1145/3590837.3590853.

[15] S. K. Sharma and A. Kumar, "Digital image transformation using outer totality cellular automata," in *Machine Intelligence Techniques for Data Analysis and Signal Processing*, D. S. Sisodia, L. Garg, R. B. Pachori, and M. Tanveer, Eds. Singapore: Springer, 2023, pp. 851–858.

[16] S. Sharma, "Brain tumor segmentation via outer totality cellular automata," *ECS Trans.*, vol. 107, no. 1, pp. 6465–6472, Apr. 2022, doi: 10.1149/10701.6465ecst.

[17] P. Xu, J. Ding, H. Zhang, and H. Huang, "Discernible image mosaic with edge-aware adaptive tiles," *Comput. Vis. Media*, vol. 5, no. 1, pp. 45–58, Mar. 2019, doi: 10.1007/s41095-019-0130-7.

[18] K. Hussain, S. Rahman, M. M. Rahman, S. M. Khaled, M. A.-A. Wadud, M. A. H. Khan, and M. Shoyaib, "A histogram specification technique for dark image enhancement using a local transformation method," *IPSJ Trans. Comput. Vis. Appl.*, vol. 10, no. 1, pp. 1–11, Feb. 2018, doi: 10.1186/s41074-018-0040-0.

[19] C. Baby Sherin and L. Mredhula, "A novel method for edge detection in images based on particle swarm optimization," *J. Phys., Conf.*, vol. 787, Jan. 2017, Art. no. 012012, doi: 10.1088/1742-6596/787/1/012012.

[20] Y. Wu, H. Zhang, Y. Li, Y. Yang, and D. Yuan, "Video object detection guided by object blur evaluation," *IEEE Access*, vol. 8, pp. 208554–208565, 2020.

[21] U. A. Usmani, J. Watada, J. Jaafar, I. A. Aziz, and A. Roy, "A reinforcement learning based adaptive ROI generation for video object segmentation," *IEEE Access*, vol. 9, pp. 161959–161977, 2021.

[22] X. He, Z. Chang, L. Zhang, H. Xu, H. Chen, and Z. Luo, "A survey of defect detection applications based on generative adversarial networks," *IEEE Access*, vol. 10, pp. 113493–113512, 2022.

[23] C. Orhei, V. Bogdan, C. Bonchis, and R. Vasiu, "Dilated filters for edge-detection algorithms," *Appl. Sci.*, vol. 11, no. 22, p. 10716, Nov. 2021. [Online]. Available: https://www.mdpi.com/2076-3417/11/22/10716

[24] Q. Hu, W. Cai, S. Xu, and S. Hu, "MRI image fusion based on sparse representation with measurement of patch-based multiple salient features," *Electronics*, vol. 12, no. 14, p. 3058, Jul. 2023. [Online]. Available: https://www.mdpi.com/2079-9292/12/14/3058

[25] T. Li, P. Zhao, Y. Zhou, and Y. Zhang, "Quantum image processing algorithm using line detection mask based on NEQR," *Entropy*, vol. 25, no. 5, p. 738, Apr. 2023. [Online]. Available: https://www.mdpi.com/1099-4300/25/5/738

[26] Y. Wu and Q. Li, "The algorithm of watershed color image segmentation based on morphological gradient," *Sensors*, vol. 22, no. 21, p. 8202, Oct. 2022. [Online]. Available: https://www.mdpi.com/1424-8220/22/21/8202

[27] W. Guo, Y. Zhang, X. Hu, T. Zhang, M. Liang, X. Yang, and H. Yang, "Region growing algorithm combined with fast peak detection for segmenting colloidal gold immunochromatographic strip images," *IEEE Access*, vol. 7, pp. 169715–169723, 2019.

[28] H. Wang, J. Cao, X. Liu, J. Wang, T. Fan, and J. Hu, "Least-squares images for edge-preserving smoothing," *Comput. Vis. Media*, vol. 1, no. 1, pp. 27–35, Mar. 2015, doi: 10.1007/s41095-015-0004-6.

[29] R. Wang, H. Yang, Z. Pan, B. Huang, and G. Hou, "Screen content image quality assessment with edge features in gradient domain," *IEEE Access*, vol. 7, pp. 5285–5295, 2019.

[30] D. Huang and Y. Hu, "Research on image smoothing diffusion model with gradient and curvature features," *IEEE Access*, vol. 7, pp. 15912–15921, 2019.

[31] H. Zheng, K. Zeng, D. Guo, J. Ying, Y. Yang, X. Peng, F. Huang, Z. Chen, and X. Qu, "Multi-contrast brain MRI image super-resolution with gradient-guided edge enhancement," *IEEE Access*, vol. 6, pp. 57856–57867, 2018.

[32] M. A. Kabir and M. R. H. Mondal, "Intensity gradient based edge detection for pixelated communication systems," *J. Eng.*, vol. 2019, no. 12, pp. 8463–8470, Dec. 2019.

[33] C. Cai, H. Meng, and Q. Zhu, "Blind deconvolution for image deblurring based on edge enhancement and noise suppression," *IEEE Access*, vol. 6, pp. 58710–58718, 2018.

[34] M. Begum and M. S. Uddin, "Implementation of secured and robust DFT-based image watermark through hybridization with decomposition algorithm," *Social Netw. Comput. Sci.*, vol. 2, no. 3, p. 221, Apr. 2021.

[35] V. Rowghanian, "Underwater image restoration with Haar wavelet transform and ensemble of triple correction algorithms using bootstrap aggregation and random forests," *Sci. Rep.*, vol. 12, no. 1, p. 8952, May 2022.

[36] T.-C. Wu, X. Wang, L. Li, Y. Bu, and D. M. Umulis, "Automatic wavelet-based 3D nuclei segmentation and analysis for multicellular embryo quantification," *Sci. Rep.*, vol. 11, no. 1, p. 9847, May 2021.

[37] K. B. Yang, J. Lee, and J. Yang, "Multi-class semantic segmentation of breast tissues from MRI images using U-Net based on Haar wavelet pooling," *Sci. Rep.*, vol. 13, no. 1, p. 11704, Jul. 2023.

[38] J. Shi, H. Jin, and Z. Xiao, "A novel hybrid edge detection method for polarimetric SAR images," *IEEE Access*, vol. 8, pp. 8974–8991, 2020.

[39] M. Suthar, H. Asghari, and B. Jalali, "Feature enhancement in visually impaired images," *IEEE Access*, vol. 6, pp. 1407–1415, 2018.

[40] L. Jiang, G. Peng, B. Xu, Y. Lu, and W. Wang, "Foreign object recognition technology for port transportation channel based on automatic image recognition," *EURASIP J. Image Video Process.*, vol. 2018, no. 1, p. 147, Dec. 2018, doi: 10.1186/s13640-018-0390-7.

[41] P. Liu, G. Wang, H. Qi, C. Zhang, H. Zheng, and Z. Yu, "Underwater image enhancement with a deep residual framework," *IEEE Access*, vol. 7, pp. 94614–94629, 2019.

[42] T. Shen, F. Huang, and L. Jin, "An improved edge detection algorithm for noisy images," in *Proc. Int. Conf. Artif. Intell. Comput. Sci.*, New York, NY, USA, Jul. 2019, pp. 84–88, doi: 10.1145/3349341.3349373.

[43] J. Tian and X. Yin, "Adaptive image enhancement algorithm based on the model of surface roughness detection system," *EURASIP J. Image Video Process.*, vol. 2018, no. 1, p. 103, Oct. 2018, doi: 10.1186/s13640-018-0343-1.

[44] A. Sabir, K. Khurshid, and A. Salman, "Segmentation-based image defogging using modified dark channel prior," *EURASIP J. Image Video Process.*, vol. 2020, no. 1, pp. 1–14, Dec. 2020.

[45] F. Peng, S. Wang, X. Wang, X. Yang, and Y. Shen, "Research on recognition for subway track based on Canny edge detection and Hough transformation," in *Proc. IEEE 6th Inf. Technology, Networking, Electronic Autom. Control Conf. (ITNEC)*, vol. 6, Feb. 2023, pp. 1664–1667.

[46] T. Shen and H. Xu, "Medical image segmentation based on transformer and HarDNet structures," *IEEE Access*, vol. 11, pp. 16621–16630, 2023.

[47] S. He and B. Jalali, "Fast super-resolution in MRI images using phase stretch transform, anchored point regression and zero-data learning," in *Proc. IEEE Int. Conf. Image Process. (ICIP)*, Sep. 2019, pp. 2876–2880.

[48] P. Xu, Z. Zhou, H. Shi, and Z. Geng, "Anisotropic phase stretch transform-based algorithm for segmentation of activated sludge phase-contrast microscopic image," *IEEE Access*, vol. 10, pp. 39518–39532, 2022.

[49] M. Challoob and Y. Gao, "A local flow phase stretch transform for robust retinal vessel detection," in *Advanced Concepts for Intelligent Vision Systems*, J. Blanc-Talon, P. Delmas, W. Philips, D. Popescu, and P. Scheunders, Eds. Cham, Switzerland: Springer, 2020, pp. 251–261.

[50] S. Meignen, N. Laurent, and T. Oberlin, "One or two ridges? An exact mode separation condition for the Gabor transform," *IEEE Signal Process. Lett.*, vol. 29, pp. 2507–2511, 2022.

[51] V. Tadic, T. Loncar-Turukalo, A. Odry, Z. Trpovski, Z. Vizvari, and P. Odry, "A note on advantages of the fuzzy Gabor filter in object and text detection," *Symmetry*, vol. 13, no. 4, 2021. [Online]. Available: https://www.mdpi.com/2073-8994/13/4/678

[52] V. Dakshayani, G. R. Locharla, P. Plawiak, V. Datti, and C. Karri, "Design of a Gabor filter-based image denoising hardware model," *Electronics*, vol. 11, no. 7, p. 1063, Mar. 2022. [Online]. Available: https://www.mdpi.com/2079-9292/11/7/1063

[53] Q. Gao, F. Yuan, F. Yuan, D. Cheng, Z. Li, and J. Pan, "GIS optical partial discharge pattarn identification based on two-dimensional Gabor transform and image features," in *Proc. Int. Conf. Adv. Electr. Equip. Reliable Operation (AEERO)*, Oct. 2021, pp. 1–5.

[54] K. Venkatachalam, S. Siuly, N. Bacanin, S. Hubálovský, and P. Trojovský, "An efficient Gabor Walsh-Hadamard transform based approach for retrieving brain tumor images from MRI," *IEEE Access*, vol. 9, pp. 119078–119089, 2021.

[55] A. Ullah, N. Ishaq, M. Azeem, H. Ashraf, N. Z. Jhanjhi, M. Humayun, T. A. Tabbakh, and Z. A. Almusaylim, "A survey on continuous object tracking and boundary detection schemes in IoT assisted wireless sensor networks," *IEEE Access*, vol. 9, pp. 126324–126336, 2021.

[56] J. C. Joubert, D. N. Wilke, and P. Pizette, "Fourier image analysis of multiphase interfaces to quantify primary atomization," *Math. Comput. Appl.*, vol. 28, no. 2, p. 55, Apr. 2023. [Online]. Available: https://www.mdpi.com/2297-8747/28/2/55

[57] J. Zak, A. Korzynska, A. Pater, and L. Roszkowiak, "Fourier transform layer: A proof of work in different training scenarios," *Appl. Soft Comput.*, vol. 145, Sep. 2023, Art. no. 110607.

[58] X.-H. Wu, R. Hu, and Y.-Q. Bao, "Block-based Hough transform for recognition of zebra crossing in natural scene images," *IEEE Access*, vol. 7, pp. 59895–59902, 2019.

[59] Q. Meng, X. Wen, L. Yuan, and H. Xu, "Factorization-based active contour for water-land SAR image segmentation via the fusion of features," *IEEE Access*, vol. 7, pp. 40347–40358, 2019.

[60] A. Chaurasia, V. S. Sharma, C. L. Chowdhary, S. Basheer, and T. R. Gadekallu, "Non-Gaussian traffic modeling for multicore architecture using wavelet based rosenblatt process," *IEEE Access*, vol. 11, pp. 38523–38533, 2023.

SANDEEP KUMAR SHARMA (Member, IEEE) received the M.Tech. and Ph.D. degrees from Rajasthan Technical University, Kota, India. He is currently an Assistant Professor with the Department of Computer and Communication Engineering, Manipal University Jaipur, India. He has published number of research papers in international and national journals/conferences. His research interests include digital image processing, AR/VR, and cellular automata.

VIJAY SHANKAR SHARMA (Member, IEEE) received the B.E., M.E., and Ph.D. degrees from the MBM Engineering College, Jodhpur, which one of the oldest engineering college of India. He is currently an Assistant Professor (Senior Scale) with the Department of Computer and Communication Engineering, Manipal University Jaipur, India. He has teaching the experience of more than ten years. He has been published 11 research papers in international and national journals/conferences. His research interests include networking and simulation, AI, ML, big data analytics, Hadoop, and the theory of computation.

AMIT CHAURASIA (Member, IEEE) received the B.Tech. degree in information technology from Uttar Pradesh Technical University, Lucknow, the M.Tech. degree in computer science from the Dayalbagh Educational Institute, Agra, in 2012, and the Ph.D. degree in computer science and engineering from the Jaypee University of Information Technology, Waknaghat, Solan, Himachal Pradesh, India, in 2020. Since 2021, he has been an Assistant Professor with the Computer and Communication Engineering Department, Manipal University Jaipur, Jaipur, Rajasthan. He is the author of 11 articles. His research interests include synthetic traffic modeling for networks-on-chip, the integration of knowledge graph with blockchain, and consensus algorithm.

SHAKILA BASHEER is currently an Assistant Professor with the Department of Information Systems, College of Computer and Information Science, Princess Nourah bint Abdul Rahman University, Saudi Arabia. She is also working on data mining, vehicular networks machine learning, blockchain, vehicular networks, and the IoT. She has more than ten years of teaching experience. She has worked and contributed in the field of data mining, image processing, and fuzzy logic. She has published more technical papers in international journals/proceedings of international conferences/edited chapters of reputed publications. Her research interest includes data mining algorithms using fuzzy logic.

CHIRANJI LAL CHOWDHARY has been with the School of Computer Science Engineering and Information Systems, Vellore Institute of Technology, since 2010, where he is currently an Associate Professor. His research interests include computer vision and image processing.

• • •